Semidefinite-programming-based optimization of quantum random access codes over noisy channels

Rafael A. da Silva [*] and Breno Marques [†]
Centro de Ciências Naturais e Humanas, Universidade Federal do ABC-UFABC, Santo André 09210-580, Brazil

(Received 23 March 2023; accepted 5 April 2023; published 28 April 2023)

There are many approaches when it comes to exploring the potential of the random access code (RAC) communication protocol. Given its versatility, the RAC is particularly useful when the communication between parties is restricted. In previous works, it has been proven that $2^{(d)} \to 1$ quantum random access codes (QRAC), in the absence of noise, outperform their classical counterpart (the $2^{(d)} \to 1$ CRAC) for any dimension d. Here, building upon these works, we showed that noisy channels can significantly decrease the performance of $2^{(d)} \to 1$ QRAC. In order to mitigate noise-driven efficiency losses, we employed the see-saw optimization algorithm with semidefinite programming (SDP) to find the best quantum encoding and decoding strategies for the QRAC given a known quantum channel.

DOI: 10.1103/PhysRevA.107.042433

I. INTRODUCTION

In quantum communication one uses quantum resources such as superposition and entanglement to enhance information transmission beyond classical limitations [1]. An example of this is the quantum random access code (QRAC), first introduced by Wiesner in 1983 [2] and rediscovered by Ambaini *et al.* [3], in which the use of quantum strategies for encoding and decoding Alice's messages improves Bob's probability of correctly accessing the information he is interested in when compared to classical strategies. In general, a QRAC involves a party, Alice, who must encode an n-dit long string into $m < n$ qudits and send to Bob, who is only interested in a random subset of the string. He must be able to retrieve this information with average probability of success $P_d > P_{\text{chance}}$, where P_{chance} represents his average probability if he would randomly guess the information. This family of QRACs can be symbolically represented as $n^{(d)} \xrightarrow{P_d} m$.

The many approaches that have been explored in the different RACs such as prepare-measure QRAC [4,5], entanglement-assisted random access code (RAC) [6], sequential QRAC [7], and QRAC with share randomness [8], and the fact that many of these works were published only recently show that this protocol is still an important research topic in quantum information, even decades after it was first proposed. Another fact that shows the relevance of the QRAC is its many important applications in quantum information in general, e.g., in quantum dimension tests [9], quantum random number generation [10,11], quantum key distribution [12], self-testing [7,13], nonclassicality tests [14], nonlocality tests [6,15], causality tests [16], quantum automata [17], connection between mutually unbiased and RAC [18], measurement incompatibility [19], and prepare-measure protocols [20].

Tavakoli *et al.* showed in Ref. [4] that, in the noiseless regime, the $2^{(d)} \xrightarrow{P_d} 1$ QRAC outperforms its classical counterpart (the CRAC) for any dimension d in terms of average probability of success. However, most systems used in the implementation of quantum communication protocols are, in both experimental and application contexts, hardly ideal. Therefore, one may not be able to completely neglect the influence of quantum noise on those systems and, consequently, on the protocol itself. In fact, accounting for quantum noise is essential for assessing possible limitations on the implementation the protocol or even its viability altogether. Quantum communication over noisy channels has been addressed in previous works for protocols such as quantum key distribution [21], quantum steganography [22], and quantum teleportation [23,24]. However, with regard to the QRACs, especially for high-dimensional generalizations such as $2^{(d)} \xrightarrow{P_d} 1$, this matter has not been treated comprehensively. To address this issue, we investigate, via simulations, how Bob's average probability of success P_d evolves with time, for a given dimension d, when the communication happens over one of the following Markovian channels: the dit flip, d-phase flip, dephasing, depolarizing, and amplitude damping channels. The simulations show that the action of these channels can reduce the efficiency of the QRACs to the point that their classical counterparts are able to perform better. We then attempted to mitigate this loss in performance by optimizing the protocol using semidefinite programming (SDP), a subfield of convex optimization that has been extensively applied for a wide range of purposes in quantum information [25–28]. It is especially well suited for our problem because our figure of merit, the quantum average probability of success, depends linearly on both the encoding states (density matrices) and decoding measurement operators, which are likewise positive semidefinite. Therefore, the task of maximizing this probability of success can be cast as an SDP.

In Sec. II we review the classical and quantum $2^{(d)} \xrightarrow{P_d} 1$ random access code protocol. In Sec. III we presented a basic overview of the theory of the open quantum system and how it relates to the concept of noisy quantum channels, and we introduce the noisy quantum channels covered in this work. In Sec. IV we applied the concepts laid out in the

[*] rafael.a@ufabc.edu.br
[†] breno.marques@ufabc.edu.br

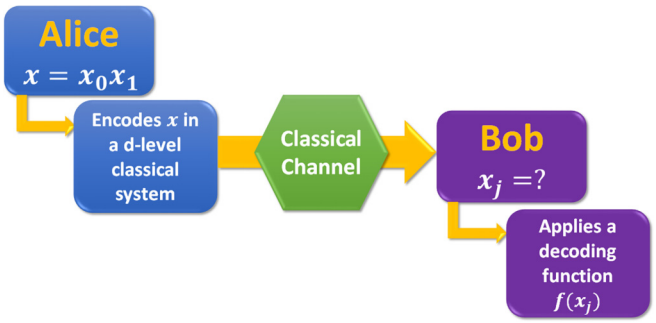

FIG. 1. Schematics of a $2^{(d)} \xrightarrow{P_d} 1$ CRAC protocol.

previous section to analyze the behavior and performance of the QRACs under those channels, and, whenever possible, we find encoding and decoding strategies, based on SDP, for mitigating noise-driven efficiency loss.

II. REVIEW OF RANDOM ACCESS CODE

A. Classical random access code

In the classical version of the $2^{(d)} \xrightarrow{P_d} 1$ RAC, Alice encodes a string $x = x_0x_1$ in one classical d-level state (see Fig. 1). The best classical strategy [4] consists of Alice always sending Bob the value of the same dit—for instance, x_0. If Bob is interested in x_0, he recovers it with probability 1, but if he is interested in x_1, he is forced to guess its value, and has a probability of $1/d$ of succeeding. This strategy has an average probability of success of

$$P^C = \frac{1}{2}\left(1 + \frac{1}{d}\right). \tag{1}$$

B. Quantum random access code

In the quantum version of the $2^{(d)} \xrightarrow{P_d} 1$ RAC, however, Alice encodes $x = x_0x_1$ in a single d-level quantum state (see Fig. 2) [4]. This state can be constructed in terms of two mutually unbiased bases (MUB). In the present work we chose the computational basis, $B_e = \{|e_l\rangle\}_{l=0}^{d-1}$ ($|e_l\rangle = |l\rangle$), and the Fourier basis, $B_f = \{|f_l\rangle\}_{l=0}^{d-1}$ ($|f_l\rangle = (1/\sqrt{d})\sum_{n=0}^{n=d-1}\omega^{ln}|n\rangle$), where $\omega = \exp 2\pi i/d$, for constructing the encoding states

$$|\psi_{x_0x_1}\rangle = \frac{1}{\sqrt{2 + (2/\sqrt{d})}}\left(|e_{x_0}\rangle + |f_{x_1}\rangle\right). \tag{2}$$

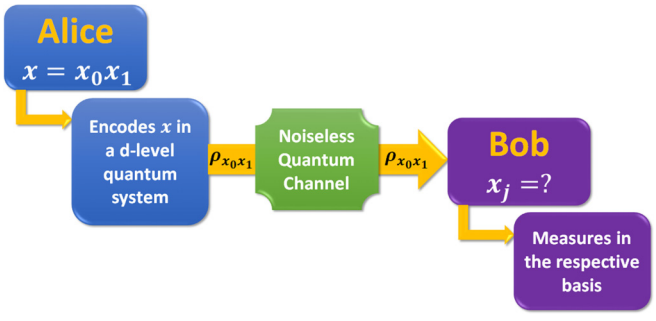

FIG. 2. Schematics of a $2^{(d)} \xrightarrow{P_d} 1$ QRAC protocol over a noiseless channel.

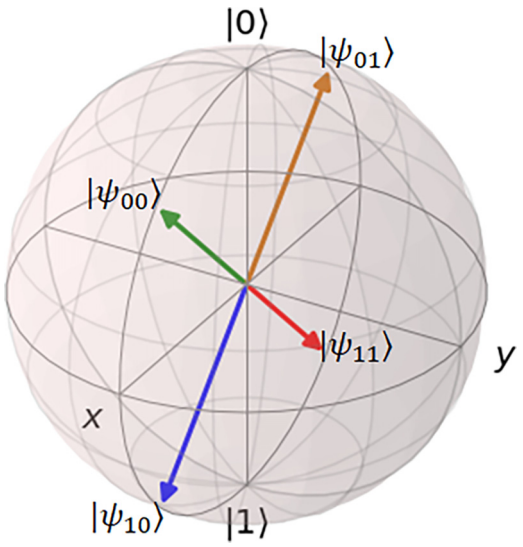

FIG. 3. We show here an example of the four encoding states ($d = 2$) plotted in the Bloch sphere. Notice that these states are symmetrically distributed in the sphere and that the projections on the z axis (computational basis) and on the x axis (Fourier basis) have the same modulus.

Whenever Bob is interested in x_0 (x_1), he performs a measurement in the basis B_e (B_f), and the average probability of success for this strategy is given by

$$\begin{aligned} P^Q &= \frac{1}{2d^2}\sum_{k=0}^{d-1}\sum_{l=0}^{d-1}\mathrm{Tr}\left\{\rho_{x_0x_1}\left(M_k^{x_0} + M_l^{x_1}\right)\right\} \\ &= \frac{1}{2}\left(1 + \frac{1}{\sqrt{d}}\right), \end{aligned} \tag{3}$$

where $\rho_{x_0x_1} = |\psi_{x_0x_1}\rangle\langle\psi_{x_0x_1}|$, $M_k^{x_0} = |e_k\rangle\langle e_k|$, and $M_l^{x_1} = |f_l\rangle\langle f_l|$. It is worth noting that the probability for any of the possible outcomes is equal to the average P^Q, regardless of the value of Alice's string $x = x_0x_1$ or which substring Bob is interested in. This happens because the magnitudes of the projections of $|\psi_{x_0x_1}\rangle$ onto B_e and B_f basis are all equal to P^Q (see Fig. 3, where this can be illustrated for $d = 2$ using the Bloch sphere). As we will see in Secs. III and IV, this symmetry can be broken when the communication occurs over noisy quantum channels, and this fact should be considered when seeking new strategies to mitigate the resulting efficiency loss.

By comparing Eqs. (1) and (3), it is straightforward to show that, under the noiseless regime, the quantum probability of success is always greater than the classical one, i.e.,

$$P^Q/P^C > 1 \quad \forall \quad d. \tag{4}$$

The ratio presented above will be used from now on as the figure of merit when comparing the performance of QRAC and CRAC.

III. NOISY QUANTUM CHANNELS

In the implementation of quantum protocols, quantum noise is often a limiting, or even prohibiting, factor when it comes to how efficiently we can perform a given task.

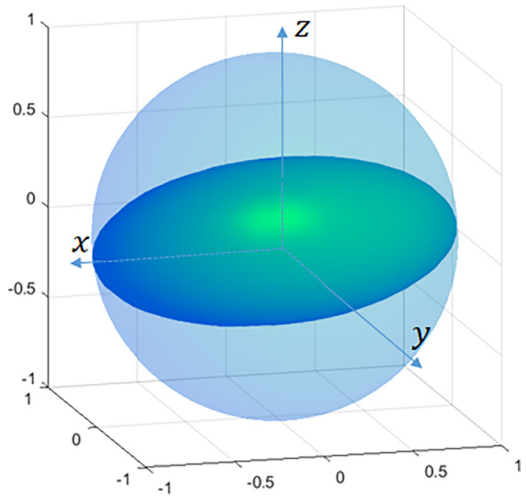

FIG. 4. Representation on the Bloch sphere of the dit flip channel for the qubit. This map conserves the probabilities of measurements in the Fourier basis but decreases the probabilities for measurements in the computational basis.

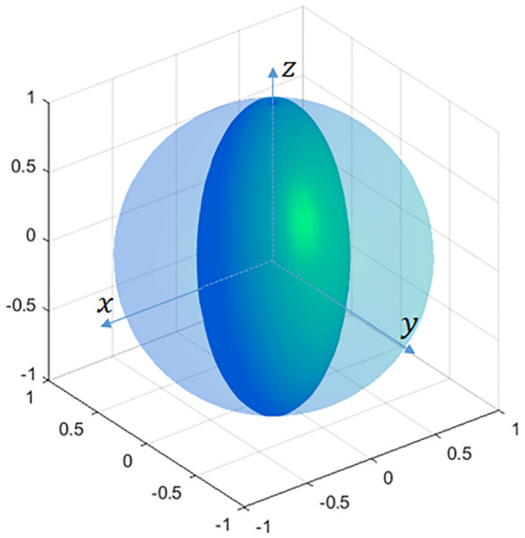

FIG. 5. Representation on the Bloch sphere of the phase flip channel for the qubit. This map conserves the probabilities of measurements in the computational basis but decreases the probabilities for measurements in the Fourier basis.

Understanding how a noisy quantum channel can affect a given protocol is essential for predicting noise-related efficiency loss. This knowledge is also essential when seeking strategies for mitigating the performance decrements without increasing the protocol complexity, e.g., without relying on quantum error correction protocols.

Quantum noise can be understood in the light of the theory of open quantum systems [29,30], which shows that this phenomenon arises from the interaction between the encoding quantum system and the environment. Furthermore, this theory characterizes noisy quantum channels, and quantum channels in general, as completely positive and trace-preserving (CPTP) maps [31] which can be mathematically represented in the Kraus' formalism as

$$\mathcal{N}(\rho) = \sum_{\nu} K_\nu \rho K_\nu^\dagger, \tag{5}$$

where K_ν are the so-called Kraus operators, which satisfy $\sum_\nu K_\nu K_\nu^\dagger = I$.

The quantum channels under consideration in this work are presented here and, as an example, the accessible states for these channels are represented in the Bloch sphere (which is only possible for $d = 2$).

A. Dit flip channel

This channel is the d-dimensional generalization of the bit flip channel whose action flips a qudit $|\mu\rangle$ (Fig. 4), with equal probability, to one of the states $|\mu \oplus 1\rangle$, $|\mu \oplus 2\rangle, \ldots,$ $|\mu \oplus d-1\rangle$, where "$\oplus$" symbolizes sum modulo d, i.e., $\mu \oplus \nu \equiv (\mu + \nu) \bmod d$. Since the dit flip channel belongs to the family of discrete Weyl's channels (DWC) [24,32], it is possible to use the Weyl's operators

$$W_{\nu\mu} = \sum_{k=0}^{d-1} \omega^{k\nu} |k\rangle\langle k \oplus \mu|, \quad \omega = \exp\{2\pi i/d\} \tag{6}$$

to write its set of Kraus operators as

$$K_\nu = \begin{cases} \sqrt{1-p}W_{0\nu}, & \nu = 0 \\ \sqrt{\frac{p}{d-1}}W_{0\nu}, & 1 \leqslant \nu \leqslant d-1. \end{cases} \tag{7}$$

B. d-Phase flip channel

The d-phase flip (phase flip, for convenience) channel is the generalization of the qubit phase flip channel (Fig. 5). It acts on a qudit $|\mu\rangle$ flipping its phase with equal probability, in one of the following ways $\omega|\mu\rangle, \omega^2|\mu\rangle, \ldots, \omega^{d-1}|\mu\rangle$, with $\omega = \exp 2\pi i/d$. The Kraus operators for this channel are given as

$$K_\mu = \begin{cases} \sqrt{1-p}W_{\mu 0}, & \mu = 0 \\ \sqrt{\frac{p}{d-1}}W_{\mu 0}, & 1 \leqslant \mu \leqslant d-1. \end{cases} \tag{8}$$

C. Depolarizing channel

The depolarizing channel is important in experimental contexts, where it is used to analyze experimental setups in which the quantum state may be lost or when working with nonideal detectors. For qudits this channel can be described as follows: ρ_S has probability p of being replaced with a completely mixed state I/d, otherwise it remains unchanged. The corresponding map is

$$\rho_S(t) = \frac{pI}{d} + (1-p)\rho_S(0), \tag{9}$$

where $p = 1 - e^{-\Gamma t}$, and Γ is the system-environment coupling constant. One interesting aspect of this channel is its symmetry (which can be visualized in Fig. 6 for $d = 2$). As a consequence, the probabilities of success for measurements in either B_e or B_f decrease with time at the same rate.

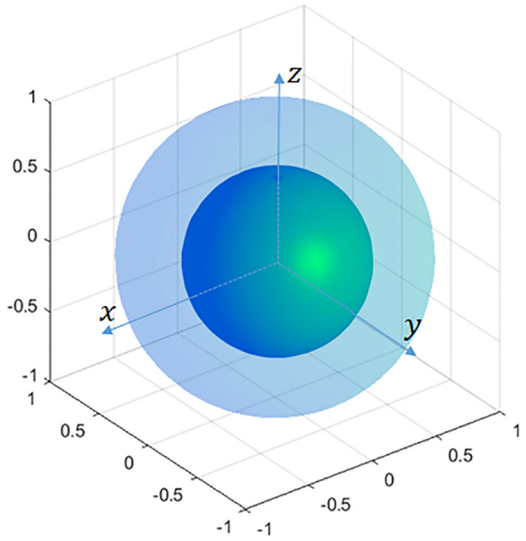

FIG. 6. Representation on the Bloch sphere of a depolarizing channel for the qubit. At $t = t_0$ the states, which are pure, lie on the surface of the sphere. As time passes and the states become mixed under the influence of noise, they now lie inside the old Bloch sphere. At a long enough time any initial state will evolve to a completely mix state represented by a single point at the center of the old Bloch sphere.

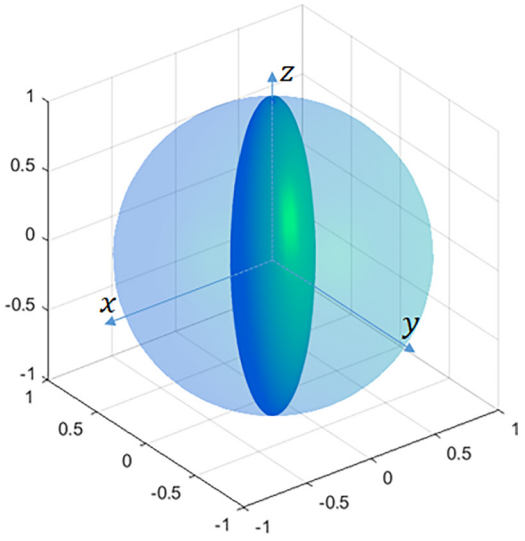

FIG. 7. Representation on the Bloch sphere of the dephasing channel for the qubit. This map "shrinks" the Bloch sphere in both the x and y direction while the poles remain unchanged. Again, this means that the probabilities of measurements in the computational basis are constant with time, but vary for measurements in the Fourier basis.

D. Dephasing channel

The dephasing channel describes a decoherence process in which quantum information is lost without loss of energy. The evolution of a qudit under this channel can be described by the equation

$$\dot{\rho}_S = \Gamma[2a^\dagger a \rho_S a^\dagger a - \{(a^\dagger a)^2, \rho_S\}], \tag{10}$$

where Γ is the dephasing system-environment coupling constant, and a and $a^\dagger$ are the annihilation and creation operators, respectively. By solving (10) one will find that the elements of the initial density matrix $\rho_S(0)$ will evolve as

$$\langle n|\rho_S(t)|m\rangle = (1-p)^{(n-m)^2}\langle n|\rho_S(0)|m\rangle. \tag{11}$$

The evolution of a qudit under this channel happens in such a manner that the probabilities for measurements in the basis B_e remain constant with time while for measurements in the basis B_f they decrease (see Fig. 7 for $d = 2$).

E. Amplitude damping channel

The amplitude damping channel is a model used to describe processes such as a quantum system losing energy to its environment, a phenomenon known as spontaneous emission [33]. In this case, it drives the system to its fundamental state $|0\rangle$ (see Fig. 8 for $d = 2$), and, as consequence, the probabilities for measurements in both bases B_e and B_f will decrease with time. This dynamics can be expressed with the Kraus operators

$$K_\nu = \begin{cases} |\nu\rangle\langle\nu| + \sqrt{1-p}\sum_{k=1}^{d-1}|k\rangle\langle k|, & \text{for} \quad \nu = 0 \\ \sqrt{p}|0\rangle\langle\nu|, & \text{for} \quad 1 \leqslant \nu \leqslant d-1. \end{cases} \tag{12}$$

IV. THE QRAC OVER NOISY CHANNELS

In the noiseless regime, the $2^{(d)} \xrightarrow{P_d} 1$ QRAC always outperforms its classical counterpart (Sec. II). As expected, we will show that this is not the case when the communication is performed over noisy quantum channels. We investigate the influence of quantum noise by considering a three-step communication process composed of encoding (state preparation), transmission, and decoding (measurement). The transmission

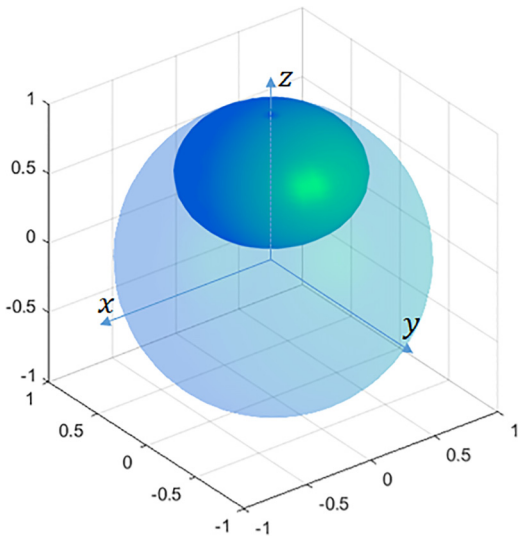

FIG. 8. Representation on the Bloch sphere of the amplitude-damping channel for a qubit. This map shrinks the Bloch sphere in the two directions of the equatorial plane, and also moves the center of the resultant ellipsoid towards the north pole, i.e., the fundamental state for spontaneous emission.

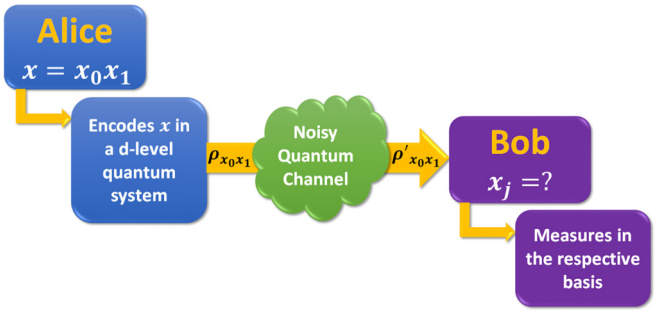

FIG. 9. Schematics of a quantum RAC protocol through a noisy channel.

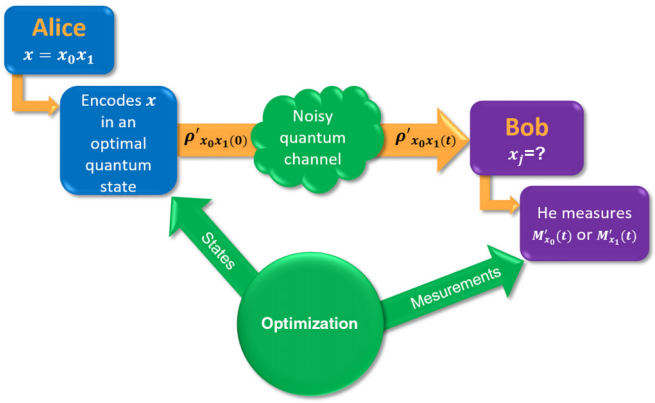

FIG. 10. Schematics of the optimized noisy QRAC protocol.

step is the only one we considered to be affected by quantum noise.

A. Scenario one: No optimization

Suppose that Alice prepares her encoding state $\rho_{x_0x_1}$ and the quantum state is sent over a noisy channel. Bob performs a measurement in either basis B_e or B_f as before (see Fig. 9 for an illustration). Thus, his average probability of success is given by

$$P^Q(t) = \frac{1}{2d^2}\sum_{k=0}^{d-1}\sum_{l=0}^{d-1}\mathrm{Tr}\left\{\rho_{x_0x_1}(t)\left(M_k^{x_0}+M_l^{x_1}\right)\right\}, \tag{13}$$

where $\rho_{x_0x_1}(t)$ is the quantum state received. The ratio

$$P^Q(t)/P^C$$

can be used to evaluate how the QRAC performance changes as a function of time in comparison to the CRAC. An important parameter is the time t_c for which $P^Q(t_c)/P^C = 1$, which marks the point in time after which the QRAC loses its advantage over the CRAC. We display this point (as Γt_c for convenience) for different values of d for $2^{(d)} \xrightarrow{P_d} 1$ QRACs and for each noisy channel in Table I.

At first glance, the results compiled in Table I seem to suggest that reaching the critical point t_c is inevitable. In fact, this is actually true when, despite the presence of quantum noise, we keep our encoding and decoding strategy fixed and based on the bases B_e and B_f. Our main goal in this work is finding flexible encoding and decoding strategies that are fine tuned for each noisy quantum channel in order to minimize performance losses. In the following section we discuss how we applied this strategy.

TABLE I. Here we display the values of Γt_c, where t_c is such that $P^Q(t_c)/P^C = 1$, at different dimensions d and for each noisy quantum channel.

Channel	$d=2$	$d=3$	$d=4$	$d=5$	$d=6$	$d=7$
Dit flip	0.35	0.44	0.47	0.48	0.47	0.46
d-Phase flip	0.34	0.45	0.46	0.48	0.46	0.46
Dephasing	0.88	0.48	0.28	0.18	0.12	0.09
Amplitude damping	0.47	0.32	0.24	0.18	0.15	0.12
Depolarizing	0.35	0.31	0.29	0.27	0.25	0.24

B. Scenario two: SDP-based optimization

The best strategy can be found for a QRAC when we take into account that $P^Q(t)$ does not depend only on the type of noise but also depends on whether or not the encoding states and decoding measurements are well adjusted to mitigate the noise channel effects. Therefore, choosing a good encoding requires anticipating the transformations that the channel may realize on the input states, and, whenever possible, optimize for the states that are least affected by them. Likewise, the decoding measurements should also reflect these channel-induced transformations. This paradigm is illustrated in Fig. 10.

The optimal encoding and decoding are determined by maximizing $P^Q(t)$. We formulated this optimization problem in terms of two interdependent SDP subproblems:

$$\begin{cases} \textbf{max} & P^Q(t) \\ \textbf{s.t.}: & \mathrm{Tr}\left\{\rho'_{x_0x_1}(t)\right\} = 1, \\ & \rho'_{x_0x_1}(t) \succcurlyeq 0, \end{cases} \tag{14}$$

and

$$\begin{cases} \textbf{max} & P^Q(t) \\ \textbf{s.t.}: & \sum_{k=0}^{d-1} M_k'^{x_0}(t) = \sum_{l=0}^{d-1} M_l'^{x_1}(t) = I, \\ & M_k'^{x_0}(t) \succcurlyeq 0, \\ & M_l'^{x_1}(t) \succcurlyeq 0, \end{cases} \tag{15}$$

where $P^Q(t)$ is given by Eq. (13), the symbol $\succcurlyeq 0$ stands for positive semidefinite, and s.t. means subject to, which states the constraints used in the optimization. In order to obtain the optimal solutions for both the encoding states and decoding measurements, the optimization was conducted using the see-saw method [34]. For every time t, in our first iteration we considered the MUB-based decoding measurements $M_k'^{x_0}(t) = |e_k\rangle\langle e_k|$ and $M_l'^{x_1}(t) = |f_l\rangle\langle f_l|$ as our starting point. They were used for finding the initial solution for the states $\rho'_{x_0x_1}(t)$, by solving the SDP described in Eq. (14). Next, we fixed the initial solution for the states $\rho'_{x_0x_1}(t)$ as the constants of our problem, and they were then used for finding the initial solution for the decoding measurements $M_k'^{x_0}(t)$ and $M_l'^{x_1}(t)$, by solving the SDP described in Eq. (15). In the next iterations this process continued in a similar fashion, except that $M_k'^{x_0}(t)$ and $M_l'^{x_1}(t)$ (at the starting point) were not based on the MUB

B_e and B_f anymore but were instead updated to be equal to the ones from the solution of the SDP in Eq. (15) from the last iteration. This process was repeated until the value of $P^Q(t)$ ceased to improve above a chosen threshold. We ran this algorithm inPYTHON 3.9 utilizing theQUTIP library for quantum mechanics operations andPICOS PYTHON API for the SDP optimization usingCVXOPT as our solver.

It is worth mentioning that we tried other ways of initializing the algorithm at the first iteration that do not involve the computational and Fourier bases. In one of our attempts, we ran the algorithms several times using a random pair of MUB and the results were indistinguishable from the one using simply the bases B_e and B_f. We also ran several experiments employing random bases that were not MUB and again there were no changes in the final results.

In Fig. 11(a) we display the values of the parameter p for which $P^Q(p)/P^C = 1$ as a function of the dimension for each of the five noisy channels when the QRAC is not optimized. Similarly, in Fig. 11(b) we display the data for the optimized version of the QRAC. The closer to unity this parameter is, the better the performance of the QRAC is in comparison to the CRAC. In fact, $p = 1$ here means that the QRAC always performs at least as well as the CRAC. Therefore, a comparison of these two graphs reveals that optimization can help to recover the supremacy, which was lost due to noise, of QRAC over its classical counterpart when the noisy channels in question are the dit flip, d-phase flip, and dephasing channels. However, for the amplitude damping and dephasing channels no improvements were found. In Fig. 11(c) we show, for each one of the five channels, how much larger the values of p in Fig. 11(b) are compared to those in Fig. 11(a), as a function of the dimension, which expresses the relative gain achieved by the optimization. Notice, for instance, that the relative gain tends to be the greatest for the dephasing channel case, especially for higher dimensions.

In graphs (a) and (b) of Figs. 12–14 the continuous lines represent the evolution of the ratio P^Q/P^C as a function of Γt when the QRAC is not optimal, while the dashed lines represent the optimized case for the dit flip, phase flip, and dephasing channels, respectively. A comparison of the dashed and continuous lines shows that the optimization substantially improved the values of P^Q/P^C overall. It provided an advantage even for lower values of Γt, and, for greater values, it guaranteed that the performance of the QRAC is greater or equal to that of the CRAC. Particularly, for the dit flip and phase flip channel, it is worth noting that for $d = 2$ and $t \to \infty$ ($p = 1$), the value of P^Q/P^C for the optimal QRAC approaches the value it had for $t = 0$ (or the noiseless QRAC), something that does not happen when the QRAC is not optimized. This happens because at this limit the action of the dit flip and phase flip channels completely flips the state, and the optimal decoding measurements are the ones that take this fact into account (for a visual insight see Fig. 16). Therefore, keeping the measurements fixed in this situation is detrimental to the performance of the protocol. Moreover, the optimization makes the QRAC more robust to high-dimensional dephasing noise, which tends to be greater the higher the dimension. In graphs (c) of Figs. 12–14 we display how many times the value of the optimal P^Q/P^C ratio is greater than the nonoptimal one as a function of Γt, which represents the gain

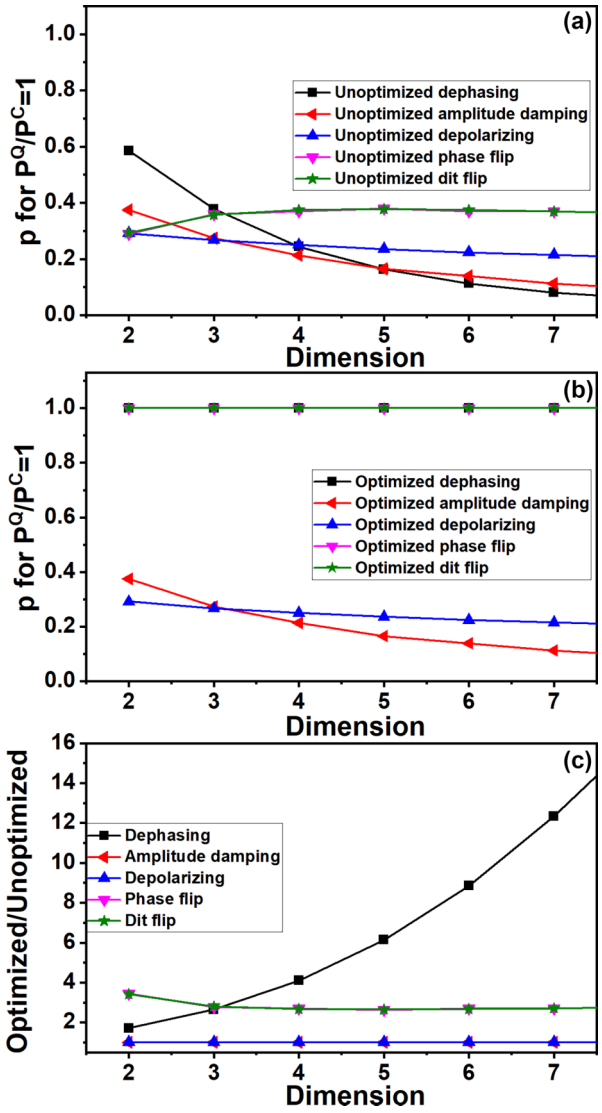

FIG. 11. (a) Values of the parameter p for which $P^Q(p)/P^C = 1$ as a function of the dimension for each of the five noisy channels when the QRAC is not optimized. (b) The same as (a), but for the optimized QRAC. To construct these graphs, for each dimension $2 \leqslant d \leqslant 7$, we ran the optimization algorithm for every $0 \leqslant p \leqslant 1$, and then looked at the evolution of average probability of success $P^Q(p)$ (i.e., as a function of the parameter p) and selected the value of p that satisfies $P^Q(p) = P^C$. The closer to unity this parameter is, the better the performance of the QRAC is in comparison to the CRAC. In fact, $p = 1$ here means that the QRAC always performs at least as well as the CRAC. Notice that in (a) we have $p < 1$ for all five channels regardless of the dimension d. However, in (b) the lines representing the dephasing, dit flip, and d-phase flip channels have $p = 1$ [in contrast to $p < 1$ in (a)], which means the optimization, in this case, guarantees a performance as least as good as the classical one, as opposed to the QRAC eventually losing its advantage over the CRAC as (a) implies. Note that the lines representing the amplitude damping and depolarizing channels in (b) are identical to those in (a), because no improvement was achieved using this particular optimization method. (c) Visualization, for each of the five channels, of how much larger the values of p in (b) are compared to those in (a), as a function of the dimension, which expresses the relative gain achieved by the optimization.

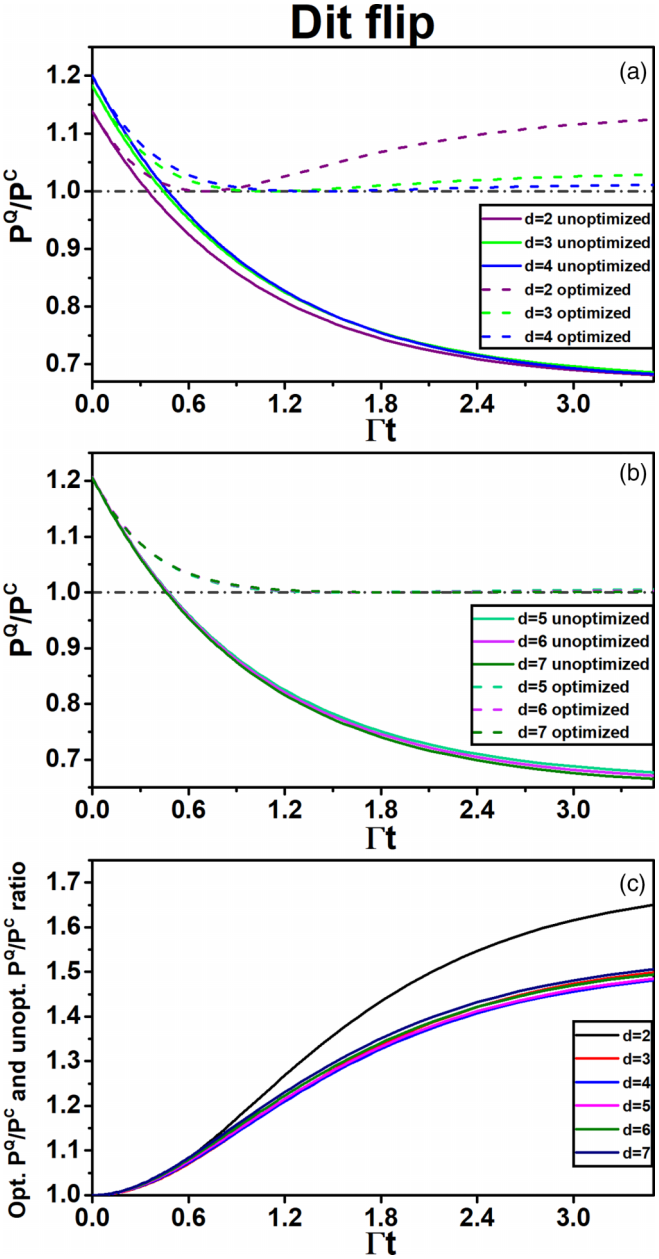

FIG. 12. (a and b) The $2^{(d)} \to 1$ QRAC, for each dimension $2 \leqslant d \leqslant 7$, over the dit flip channel. The continuous lines show the $P^Q(\Gamma t)/P^C$ ratio (i.e., as a function of the time parameter Γt) when no optimization was applied to the protocol, and the dashed lines represent this ratio when we applied SDP-based optimization to the QRAC. The dashed lines in (a) and (b) are the result of executing the algorithm for every time t. To build the continuous lines no optimization was applied, and the decoding and encoding were fixed for every time t and based on the MUB B_e and B_f. (c) To construct this graph, we consider the ratio of the values of P^Q/P^C for the optimized QRAC to the values P^Q/P^C for nonoptimized QRAC and plot it as a function of Γt. This ratio expresses the relative gain achieved by the optimization. For instance, the relative gain in this case is the greatest for $d = 2$ and decreases with the dimension.

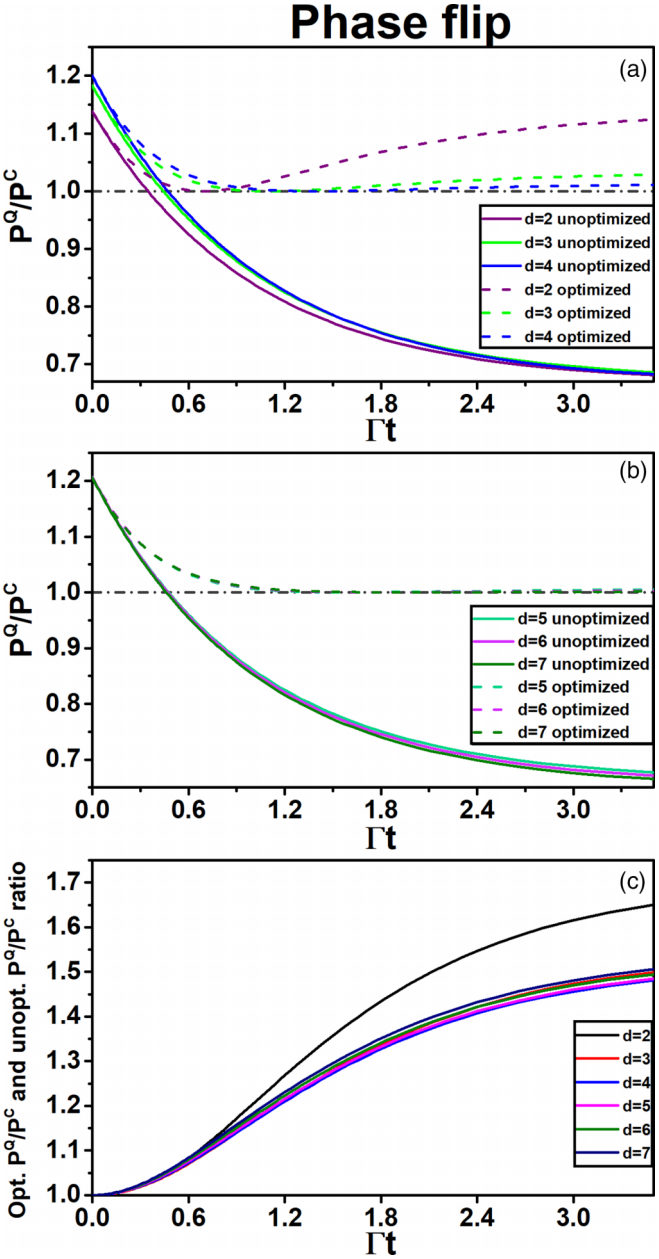

FIG. 13. (a and b) The $2^{(d)} \to 1$ QRAC, for each dimension $2 \leqslant d \leqslant 7$, over the d-phase flip channel. The continuous lines show the $P^Q(\Gamma t)/P^C$ ratio (i.e., as a function of the time parameter Γt) when no optimization was applied to the protocol, and the dashed lines represent this ratio when we applied SDP-based optimization to the QRAC. The dashed lines in (a) and (b) are the result of executing the algorithm for every time t. To build the continuous lines no optimization was applied, and the decoding and encoding were fixed for every time t and based on the MUB B_e and B_f. (c) To construct this graph, we consider the ratio of the values of P^Q/P^C for the optimized QRAC to the values P^Q/P^C for nonoptimized QRAC and plot it as a function of Γt. This ratio expresses the relative gain achieved by the optimization. For instance, the relative gain in this case is the greatest for $d = 2$.

from optimization, which increases with Γt. For the dephasing channel, it increases with the dimension, but for the dit flip and phase flip channels, it varies less with d and has the highest value for $d = 2$. Figures 16 and 15 are visual representations of the optimal encodings and how they evolve with parameter p.

As we discussed in Sec. II, the optimal noiseless QRAC strategy is based on MUB: the information is encoded in the

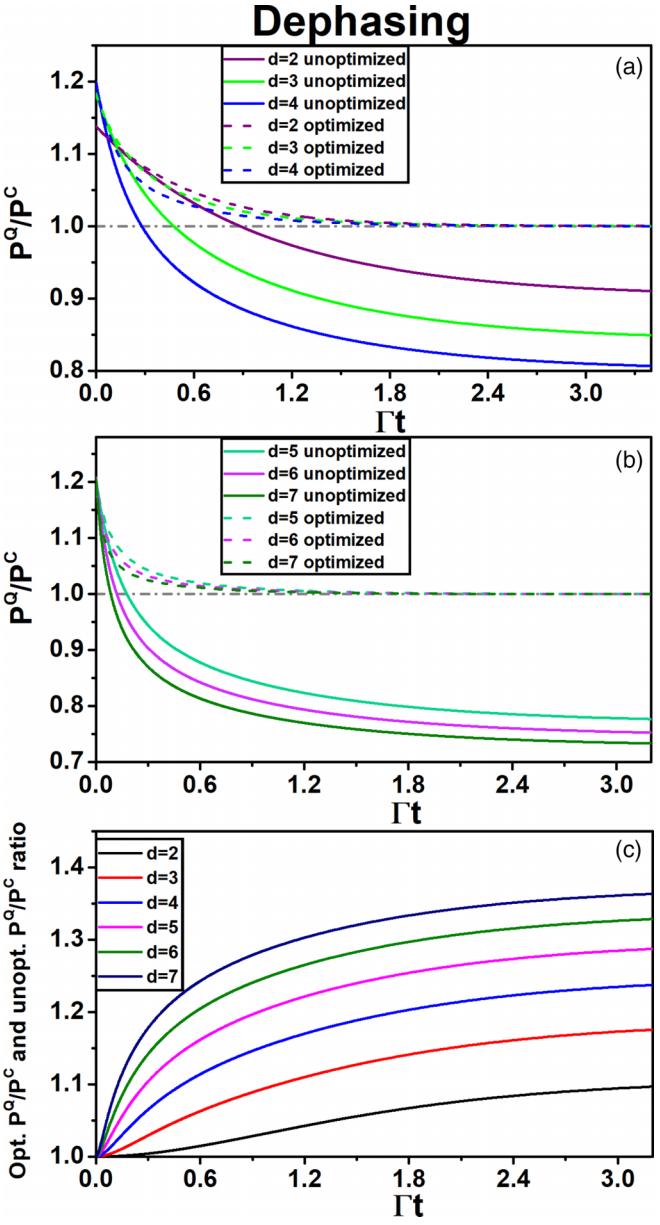

FIG. 14. (a and b) The $2^{(d)} \to 1$ QRAC, for each dimension $2 \leqslant d \leqslant 7$, over the dephasing channel. The continuous lines show the $P^Q(\Gamma t)/P^C$ ratio (i.e., as a function of the time parameter Γt) when no optimization was applied to the protocol, and the dashed lines represent this ratio when we applied SDP-based optimization to the QRAC. The dashed lines in (a) and (b) are the result of executing the algorithm for every time t. To build the continuous lines no optimization was applied, and the decoding and encoding were fixed for every time t and based on the MUB B_e and B_f. (c) To construct this graph, we consider the ratio of the values of P^Q/P^C for the optimized QRAC to the values P^Q/P^C for nonoptimized QRAC and plot it as a function of Γt. This ratio expresses the relative gain achieved by the optimization. For instance, the relative gain in this case is the greatest for $d = 7$.

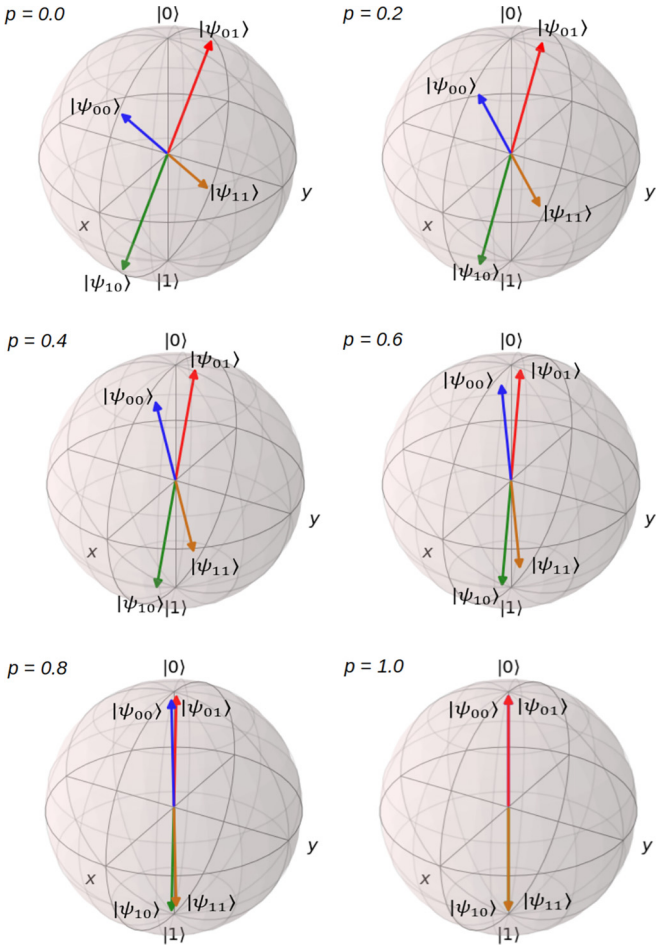

FIG. 15. Here we display on the Bloch sphere the optimal encoding states for the dephasing channel (for $d = 2$) and for different values of the parameter p. Notice that the new optimal encoding is not fixed anymore or strictly based on MUB. Instead, it changes with the parameter p as a way to compensate for the action of channel. However, the larger the value of p, the more ineffectively we can counteract this action. Ultimately, when $p = 1$, our encoding states lie on the z axis, which allows Alice to encode only one of the bits, forcing Bob to guess the other, just as in classical RAC. Therefore, in the worst case the optimization produces results that are at least as good as the classical ones.

superposition of states coming from two MUB, and it is decoded by measuring in either one of those bases, depending on which letter Bob is interested in. However, when optimizing the strategy in the presence of a noisy quantum channel, the resulting encoding and decoding are not based exclusively on MUB anymore. For instance, the optimal decoding measurements for the dit flip and d-phase flip channels are based on MUB for all time t, however the encoding states are not necessarily based on a superposition of two MUB. For the dephasing, the encoding and the decoding change, but the computational bases is preserved as one of the measurement bases. Therefore, indiscriminately relying on MUB in such a scenario can lead to suboptimal encoding and decoding strategies. In this work we focused on the QRAC protocol, however these findings might be true for other prepare-measure protocols.

Given the success of the optimization for the dit flip, d-phase flip, and dephasing channels, a natural question is why it failed for the depolarizing and amplitude damping channels. First, it should be emphasised that our approach only works when better encoding states and better decoding

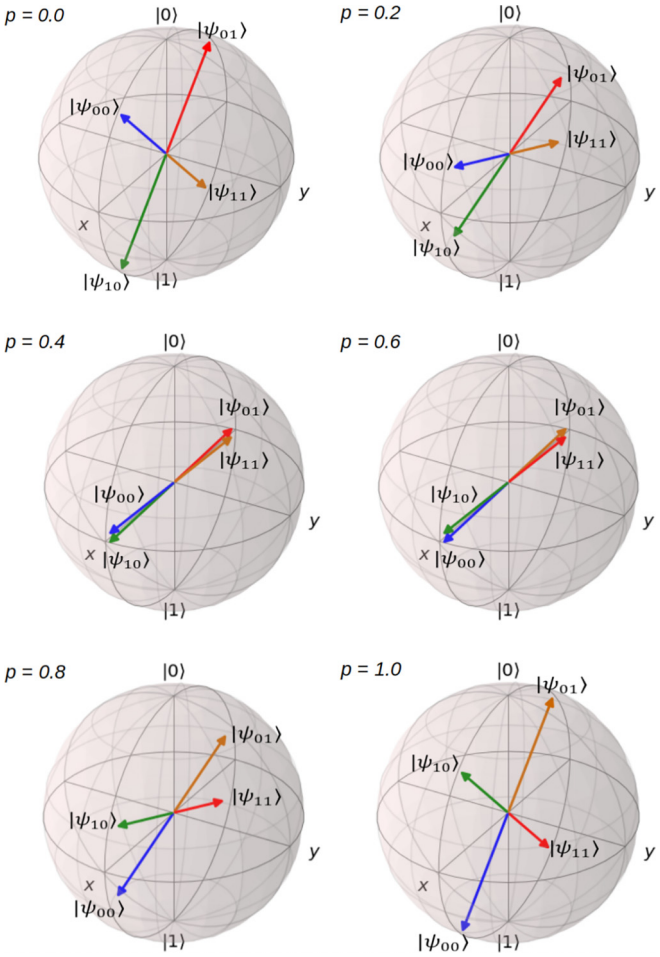

FIG. 16. Here we display on the Bloch sphere the optimal encoding states for dit flip channel (for $d = 2$) and for different values of the parameter p. Similarly to the dephasing case, the optimal encoding here is not always based on MUB. As p increases, the encoding states approach the x axis, and for $p = 0.5$ they lie on exactly on it. This marks the point where the encoding is the least efficient and is equivalent to classical encoding. However, for $p > 0.5$, we are actually able to find increasingly more efficient encoding states, and in the limit of $p \to 1$, the optimal states are again based on MUB. Notice, for instance, that the encoding states for $p = 1$ are a mirror image of those for $p = 0$. This means that, for $p = 1$, the channel output states will identical to those for $p = 0$. So we can decode Alice's string using the same decoding measurements in both cases. However, if we had not flipped the input states (no optimization) and used the same decoding strategy, it would result in a poor performance, as the graphs of Fig. 12 suggest. This is an example of how employing a dynamical rather than a fixed encoding/decoding strategy can help improve performance when certain characteristics of the channel can be used in our favor.

measurements exist. The depolarizing channel transforms the qudit symmetrically (this can intuitively be seen in Fig. 6 for $d = 2$), and as consequence, the probabilities of measurement outcomes will decrease symmetrically with time t for any decoding basis and for any encoding state. Therefore, the encoding and decoding using B_e and B_f already lead to the best $P^Q(t)$ one can possibly achieve for this channel. The amplitude damping channel, however, drives the qudit to the fundamental state, which makes the probability of success for decoding some values of x_0 or x_1 increasingly small as time passes, given that the possibility to communicate through this channel vanishes in time. Despite this, however, the fact that we fail to optimize the QRAC under the amplitude damping channel for finite t using the approach presented in this work does not necessarily imply it cannot be accomplished. Therefore, this matter should be the subject of further investigation.

V. CONCLUSION

In this work we reviewed the concept of the $2^{(d)} \to 1$ random access code in both its classical and quantum versions and presented the generalized quantum maps to describe well-known noisy channels for any discrete dimension d. We built upon this work by incorporating the theory of open quantum systems to understand how the most common noisy channels affect the performance of QRAC, and we showed how the SDP-based see-saw method can be used to optimize the protocol even in the presence of noise-induced losses. The method presented here can be useful for many other quantum communication protocols when it is desirable to improve their effectiveness without the need of extra quantum resources. This work opens new possibilities to investigate similar methods in the context of quantum communication and quantum computation protocols when the type of noisy channel is known. Even though we focused on single-qudit encoding in this work, we suspect that this method can also be used with more than a single quantum system or in different types of quantum information protocols that are not strictly prepare-measure protocols. Lastly, although the present work was meant to follow an SDP-based approach, we strongly believe that an analytical model would be very insightful and should be the subject of further investigation.

ACKNOWLEDGMENTS

R.A.S. acknowledges support from the Brazilian agency CAPES and CNPq. B.M. acknowledges partial support from the Brazilian National Institute of Science and Technology of Quantum Information (CNPq-INCT-IQ, Grant No. 465469/2014-0), CAPES/PrInt Process No. 88881.310346/2018-01.

[1] G. Brassard, Foundations Phys. **33** 1593 (2003).
[2] S. J. Wiesner, Conjugate coding, SIGACT News **15** 78 (1983).
[3] A. Ambainis, A. Nayak, A. Ta-Shma, and U. Vazirani, Dense Quantum Coding and a Lower Bound for 1-Way Quantum Automata, in *Proceedings of the 31st Annual ACM Symposiumon Theory of Computing* (1999), pp. 376–383.
[4] A. Tavakoli, A. Hameedi, B. Marques, and M. Bourennane, Quantum Random Access Codes Using Single d-Level Systems, Phys. Rev. Lett. **114**, 170502 (2015).
[5] O. Liabøtrø, Improved classical and quantum random access codes, Phys. Rev. A **95**, 052315 (2017).

[6] A. Tavakoli, B. Marques, M. Pawlowski, and M. Bourennane, Spatial versus sequential correlations for random access coding, Phys. Rev. A **93**, 032336 (2016).

[7] K. Mohan, A. Tavakoli, and N. Brunner, Sequential random access codes and self-testing of quantum measurement instruments, New J. Phys. **21**, 083034 (2019).

[8] A. Ambainis, D. Leung, L. Mancinska, and M. Ozols, Quantum random access codes with shared randomness, arXiv:0810.2937v3.

[9] J. Ahrens, P. Badziag, M. Pawlowski, M. Zukowski, and M. Bourennane, Experimental Tests of Classical and Quantum Dimensionality, Phys. Rev. Lett. **112**, 140401 (2014).

[10] H. W. Li, M. Pawlowski, Z. Q. Yin, G. C. Guo, and Z. F. Han, Semi-device-independent randomness certification using $n \to 1$ quantum random access codes, Phys. Rev. A **85**, 052308 (2012).

[11] P. Mironowicz, A. Tavakoli, A. Hameedi, B. Marques, M. Pawlowski, and M. Bourennane, Increased certification of semi-device independent random numbers using many inputs and more post-processing, New J. Phys. **18**, 065004 (2016).

[12] M. Pawłowski and N. Brunner, Semi-device-independent security of one-way quantum key distribution, Phys. Rev. A **84**, 010302(R) (2011).

[13] A. Tavakoli, J. Kaniewski, T. Vertesi, D. Rosset, and N. Brunner, Self-testing quantum states and measurements in the prepare-and-measure scenario, Phys. Rev. A **98**, 062307 (2018).

[14] A. Ambainis, M. Banik, A. Chaturvedi, D. Kravchenko, and A. Rai, Parity oblivious d-level random access codes and class of noncontextuality inequalities, Quant. Info. Proc. **18**, 111 (2019).

[15] A. Tavakoli, J. Pauwels, E. Woodhead, and S. Pironio, Correlations in entanglement-assisted prepare-and-measure scenarios, PRX Quantum **2**, 040357 (2021).

[16] M. Pawłowski, T. Paterek, D. Kaszlikowski, V. Scarani, A. Winter, and M. Zukowski, Information causality as a physical principle, Nature (London) **461**, 1101 (2009).

[17] A. Ambainis, A. Nayak, A. Ta-Shma, and U. Vazirani, Dense quantum coding and quantum finite automata, J. ACM **49**, 496 (2002).

[18] E. A. Aguilar, J. J. Borkala, P. Mironowicz, and M. Pawlowski, Connections between Mutually Unbiased Bases and Quantum Random Access Codes, Phys. Rev. Lett. **121**, 050501 (2018).

[19] C. Carmeli, T. Heinosaari, and A. Toigo, Quantum random access codes and incompatibility of measurements, Europhys. Lett. **130**, 50001 (2020).

[20] J. Pauwels, A. Tavakoli, E. Woodhead, and S. Pironio, Entanglement in prepare-and-measure scenarios: Many questions, a few answers, New J. Phys. **24**, 063015 (2022).

[21] B. Qi and Charles Ci Wen Lim, Noise Analysis of Simultaneous Quantum Key Distribution and Classical Communication Scheme Using a True Local Oscillator, Phys. Rev. Appl. **9**, 054008 (2018).

[22] C. Sutherland and T. A. Brun, Quantum steganography over noisy channels: Achievability and bounds, Phys. Rev. A **100**, 052312 (2019).

[23] R. Fortes and G. Rigolin, Fighting noise with noise in realistic quantum teleportation, Phys. Rev. A **92**, 012338 (2015).

[24] A. Fonseca, High-dimensional quantum teleportation under noisy environments, Phys. Rev. A **100**, 062311 (2019).

[25] D. Cavalcanti, P. Skrzypczyk, and I. Šupić, All Entangled States can Demonstrate Nonclassical Teleportation, Phys. Rev. Lett. **119**, 110501 (2017).

[26] F. Rozpędek, T. Schiet, L. P. Thinh, D. Elkouss, A. C. Doherty, and S. Wehner, Optimizing practical entanglement distillation, Phys. Rev. A **97**, 062333 (2018).

[27] J. Åberg, R. Nery, C. Duarte, and R. Chaves, Semidefinite Tests for Quantum Network Topologies, Phys. Rev. Lett. **125**, 110505 (2020).

[28] F. Bischof, H. Kampermann, and D. Bruß, Quantifying coherence with respect to general quantum measurements, Phys. Rev. A **103**, 032429 (2021).

[29] C. Gardiner and P. Zoller, *Quantum Noise: A Handbook of Markovian and Non-Markovian Quantum Stochastic Methods with Applications to Quantum Optics* (Springer, New York, 2000).

[30] H.-P. Breuer and F. Petruccione, *The Theory of Open Quantum Systems*, 2nd ed. (Oxford University Press, New York, 2002).

[31] L. Gyongyosi and S. Imre, Properties of the Quantum Channel, Department of Telecommunications, Budapest University of Technology and Economics (2012).

[32] J. ur Rehman, Y. Jeong, J. S. Kim, and H. Shin, Holevo capacity of discrete Weyl channels, Sci. Rep. **8**, 17457 (2018).

[33] A. Salles, F. de Melo, M. P. Almeida, M. Hor-Meyll, S. P. Walborn, P. H. Souto Ribeiro, and L. Davidovich, Experimental investigation of the dynamics of entanglement: Sudden death, complementarity, and continuous monitoring of the environment, Phys. Rev. A **78**, 022322 (2008).

[34] J. C. Spall, Cyclic seesaw process for optimization and identification, J. Opt. Theory Appl. **154**, 187 (2012).